Giant Optical Response from Graphene–Plasmonic System

Pu Wang,[†] Wei Zhang,[†] Owen Liang,[†] Marcos Pantoja,[†] Jens Katzer,[‡] Thomas Schroeder,[‡] and Ya-Hong Xie[†,*]

[†]Department of Materials Science and Engineering and California Nano Systems Institute, University of California Los Angeles, Los Angeles, California 90095-1595, United States and [‡]Innovations for High Performance (IHP), Im Technologiepark 25, Frankfurt (Oder), D-15236, Germany

ABSTRACT

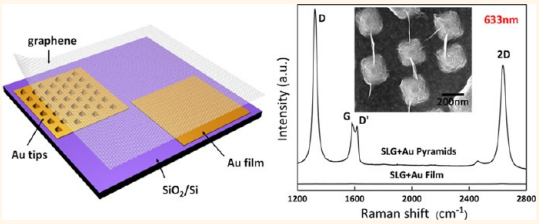

The unique properties of graphene when coupled to plasmonic surfaces render a very interesting physical system with intriguing responses to stimuli such as photons. It promises exciting application potentials such as photodetectors as well as biosensing. With its semimetallic band structure, graphene in the vicinity of metallic nanostructures is expected to lead to non-negligible perturbation of the local distribution of electromagnetic field intensity, an interesting plasmonic resonance process that has not been studied to a sufficient extent. Efforts to enhance optoelectronic responses of graphene using plasmonic structures have been demonstrated with rather modest Raman enhancement factors of less than 100. Here, we examine a novel cooperative graphene–Au nanopyramid system with a remarkable graphene Raman enhancement factor of up to 10^7. Experimental evidence including polarization-dependent Raman spectroscopy and scanning electron microscopy points to a new origin of a drastically enhanced D-band from sharp folds of graphene near the extremities of the nanostructure that is free of broken carbon bonds. These observations indicate a new approach for obtaining detailed structural and vibrational information on graphene from an extremely localized region. The new physical origin of the D-band offers a realistic possibility of defining active devices in the form of, for example, graphene nanoribbons by engineered graphene folds (also known as wrinkles) to realize edge-disorder-free transport. Furthermore, the addition of graphene made it possible to tailor the biochemical properties of plasmonic surfaces from conventional metallic ones to biocompatible carbon surfaces.

KEYWORDS: graphene · Au nanopyramids · optical response · spatially resolved Raman spectra · polarization effects

The remarkable mechanical,[1] electronic, and photonic properties[2−4] of graphene make it a promising candidate in applications ranging from biosensing[5,6] to photodetecting.[7−10] In the recent past, the combination of graphene with plasmonic nanostructures has led to an increase in efficiency of various electro-optic processes.[11] Nonetheless, the highest enhancement factor reported to date is less than 100 at the "hot spots"[12,13] of plasmonic resonance. Here we demonstrate a remarkable graphene Raman enhancement of up to 10^7 from what we believe is the cooperative plasmonic resonance of graphene on a uniquely engineered Au nanopyramid surface hereafter referred to as an Au tipped surface. The strong dependence of the Raman enhancement factor of graphene on the wavelength of the excitation laser (with the largest enhancement detected at 633 nm) lends itself to demonstrating the resonant nature of the Au tipped surface. Graphene Raman intensity mapping places the hot spots in between neighboring pyramids of atomic sharpness, indicating the cooperative nature of the resonance. In addition, a prominent D-band appeared at localized hot spots from graphene on Au tipped surfaces that is nearly absent from exactly the same piece of graphene on the immediately adjacent flat Au surface. Polarization-dependent Raman spectroscopy shows a strong 2-fold symmetry unique to the new D-band. This is in stark contrast to the G-band and 2D-band that have no observable polarization dependence. These experimental observations serve as clear evidence for the origin of the D-band being the sharp graphene folds near the apex of the Au pyramids instead of broken carbon bonds, which commonly exist at the cracks and the edges of graphene. The new D-band origin can be used as disorder-free boundaries defining the active region of electronic devices such as the channel of field effect transistors and is of significant interest for carbon electronics.

RESULTS AND DISCUSSION

Figure 1a illustrates a typical sample that consists of three regions located immediately next to one another, namely, the Au tipped surface, the flat Au surface, and the surface of flat SiO_2 of 300 nm thickness (see

* Address correspondence to yhx@ucla.edu.

Received for review April 17, 2012 and accepted June 19, 2012.

Published online June 19, 2012
10.1021/nn301694m

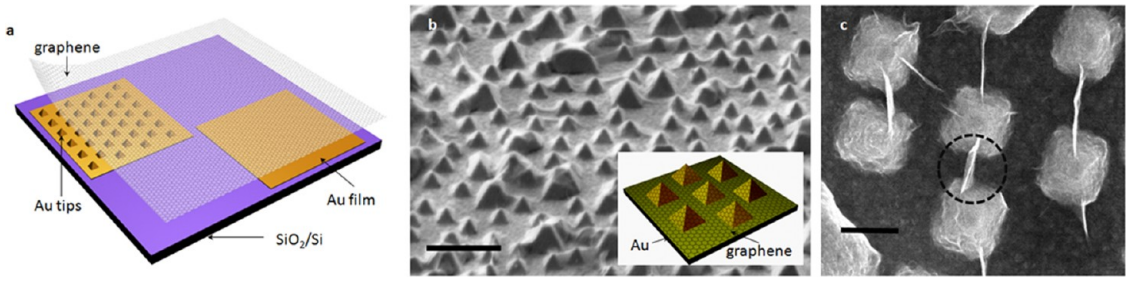

Figure 1. Graphene–Au nanopyramid (tip) structure. (a) Schematics of typical samples. (b) SEM image of graphene on Au tips; scale bar 1 μm. Inset: Schematic image of graphene on Au tips. (c) SEM image of hexagonally arranged arrays of Au tips with sharply folded graphene; scale bar 200 nm. The dotted black circle indicates a hanging graphene fold between neighboring tips.

Supporting Information). Hexagonally ordered Au nanopyramid (of ~250 nm base with radius of curvature at the apex as small as 1 nm) arrays on a continuous Au film of approximately 200 nm thickness is fabricated by nanocasting.[14] The Au tipped surface is unique in that it possesses in-plane anisotropy with wafer-scale coherency in the precise orientation and shape of individual pyramids. Uniformly single layer graphene is grown on a copper foil *via* chemical vapor deposition (CVD)[15] and subsequently transferred to cover all three regions.[16,17] The region of graphene over 300 nm SiO_2/Si is used for determining the quality of the transferred graphene. The region with graphene over flat Au is used for comparison with graphene over a tipped surface, thereby allowing for the extraction of the vibrational features (using Raman spectroscopy) due uniquely to the graphene–Au tips combination.

Figure 1b and c show typical scanning electron micrographs of graphene over a Au tipped surface. The identical shape, the precise orientation, and the non-negligible variation in the size of Au pyramids are clearly visible from Figure 1b. The nonplanar topology of the Au tipped surface necessitates folds in the graphene (Figure.1c) as it interacts with its surroundings *via* van der Waals forces. As will be discussed later, these graphene folds are believed to be the origin of a new set of D-bands in the graphene Raman spectrum.

Micro-Raman spectra of graphene[18] were obtained from three different regions using various excitation wavelengths (488, 514, 633 nm) under normal incident light (Figure 2a–c). A number of observations can be made from Figure 2: first, graphene Raman peak intensity enhancement of up to 3 orders of magnitude is present from graphene on Au tips compared to that on flat Au, providing the first evidence of the plasmonic nature of the Au tips (Figure 2d). Second, the enhancement factor is largest for the 633 nm excitation wavelength. In addition, the measured extinction spectrum[19] of the bare Au tipped region (Figure 2e) shows a maximum in extinction centered around 600 nm with a full-width at half-maximum (fwhm) of 100 nm. The combined enhancement and extinction measurements provide strong evidence of the resonant nature of the Au tipped surfaces. Third, there is a difference in the enhancement factors of about a factor of 10 between Raman intensities and the extinction magnitude (Figure 2f), with the former being larger. This is interpreted as evidence of the cooperative nature in electromagnetic field enhancement[20–22] of graphene on Au tips as the extinction spectrum was measured without graphene coverage. Finally, there appears a prominent D-band and D′-band pair (Figure 2c) that were barely visible from graphene on flat Au and on the SiO_2 region. We attribute this to the sharp graphene folds, as supported by the polarization-dependent studies to be presented below. The considerable increase of the *I*(D) to *I*(G) ratio with excitation wavelength is well known in the Raman scattering of sp^2 carbon materials.[23–25] It should be noted that although the apparent Raman enhancement factor is on the order of 1000, the actual enhancement factor is orders of magnitude higher. While the signal of conventional Raman spectra is derived from an area comparable with the excitation wavelength, Raman signals from plasmonic enhancement come predominantly from electromagnetic field concentration that is extremely localized to typically a nanometer region.[26] This difference in the area of the Raman signals leads to the actual enhancement factor of up to 10^7 times (see Supporting Information).

We employ spatially resolved Raman[27] to examine the distribution of hot spots as shown in Figure 3. The important role of the Au tips in the formation of hot spots is evident as the location of hot spots for the D-band, G-band, and 2D-band are all within the same proximity. However, the exact location of the three bands reveals clear differences, provoking an in-depth examination. Within the diffraction-limited spatial resolution of the 633 nm wavelength laser, the G-band and 2D-band hot spots coincide with one another. They are clearly located in between neighboring Au tips away from graphene folds (Figure 3b,c). Being located over a region of flat Au of ~200 nm in length (*e.g.*, the dotted circle in Figure 3b), such hot spots are not expected on bare Au tip arrays on the basis of a well-established understanding from electromagnetic field modeling.[28] We thus attribute it as evidence of cooperative behavior between the semimetallic

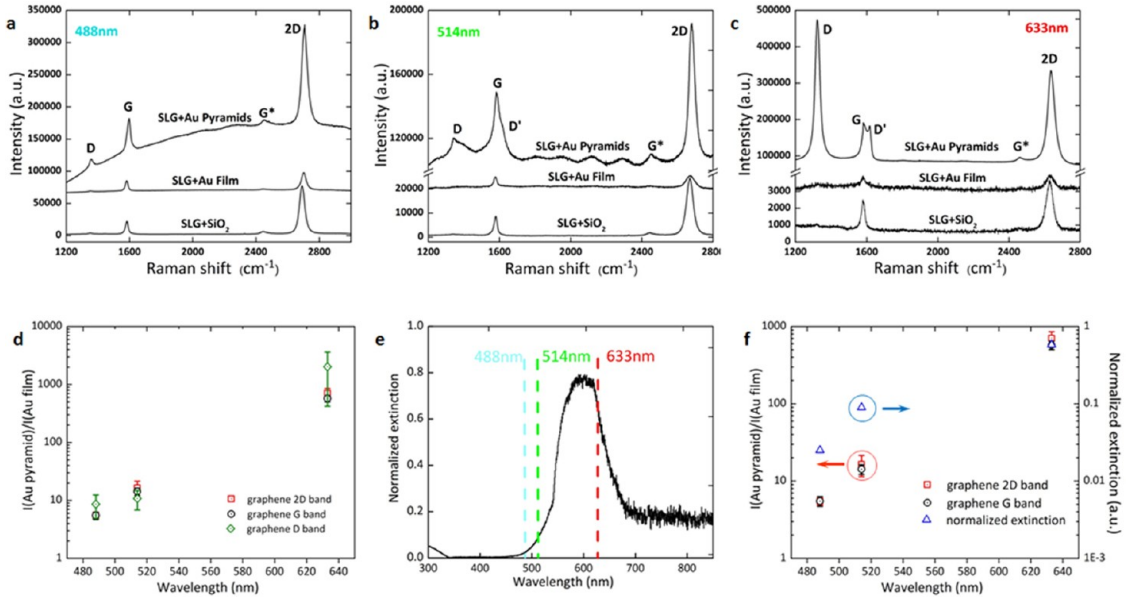

Figure 2. Raman spectra of graphene on a Au tipped structure and the wavelength selectivity. (a−c) Graphene Raman spectra measured from various surfaces (Au tips, flat Au, and SiO_2) at three different excitation wavelengths: (a) 488 nm, (b) 514 nm, (c) 633 nm. (d) Ratios of the intensity of graphene D, G, and 2D peaks measured on the Au tipped region to those measured on flat Au regions. The ratios in semilog scale are plotted as a function of the excitation wavelength. (e) Extinction spectrum of Au tips. The three excitation wavelengths of 488, 514, and 633 nm are marked with blue, green, and red dotted lines, respectively. (f) Normalized extinction at 488, 514, and 633 nm contrasted with the G and 2D intensity ratio.

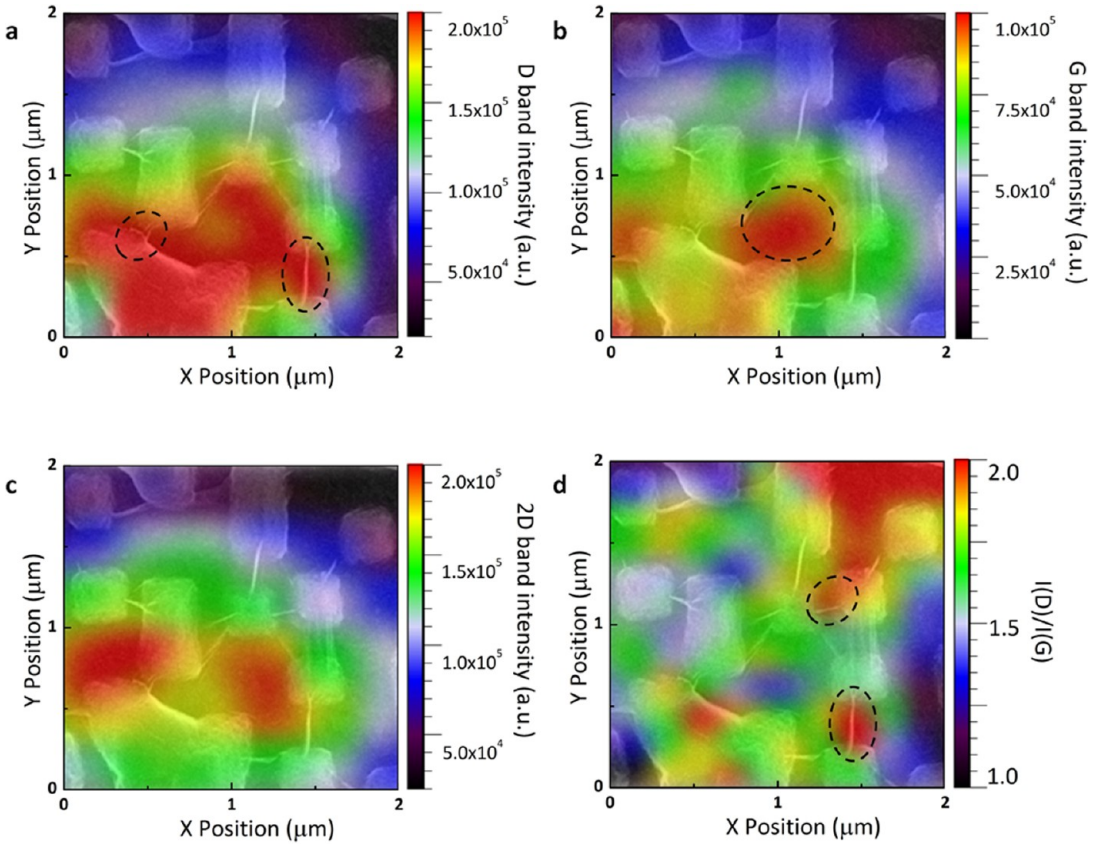

Figure 3. 2 μm × 2 μm graphene micro-Raman (633 nm) mapping data superimposed on the SEM images of the same regions. (a) D-band intensity; (b) G-band intensity; (c) 2D-band intensity; and (d) D/G intensity ratio.

graphene (with its presence altering the spatial distribution of the electromagnetic field and thus the location of the observed hot spots) and the underlying Au tips. In contrast, additional hot spots of D-bands are

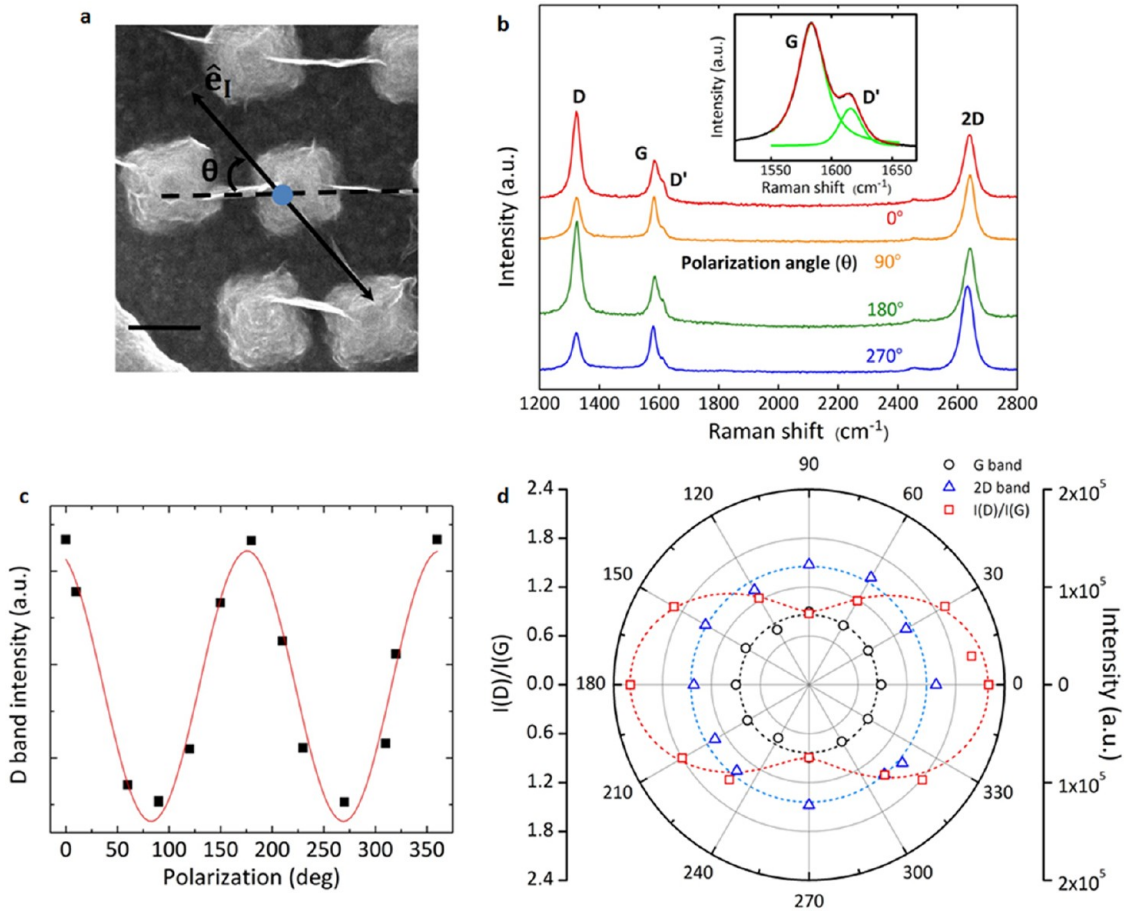

Figure 4. D-Band polarization dependence from Raman (633 nm) spectra of graphene on the Au tip region. (a) SEM image of the measured region showing sharp graphene folds with θ measuring the polarization angle between the fold direction (dotted line) and the incident electric field ($\hat{e}_I$) (solid line); scale bar 200 nm. (b) Raman spectra obtained with a polarization angle θ of 0°, 90°, 180°, and 270°. Inset: Curve-fitting results of the G- and D′-bands. (c) Polarization-dependent D-band intensity of graphene folds. Black squares: measured data; red line: $\cos^2\theta$ fit. (d) Polar plot of the *I*(D)//(G) ratio; G-band and 2D-band intensity of graphene folds as a function of polarization angle θ. Measured data: black circles, G-band intensity; blue triangles, 2D-band intensity; red squares, *I*(D)//(G) ratio. Red dotted line: $\cos^2\theta$ fit.

observed coinciding with sharp graphene folds, as highlighted by dotted circles in Figure 3a. These new D-band hot spots possess strong polarization dependence, pointing to their plausible physical origin, as will be discussed in the next section. Figure 3d shows the mapping of the ratio of D-bands to G-bands. It illustrates a clear trend of stronger D-bands where graphene folds are. It also shows an anomalous increase in D-band intensity across the entire sample area studied in comparison to graphene on SiO_2, where $I(D):I(G) \ll 1$. This point will be addressed in the discussion below.

We have observed for the first time (to our knowledge) evidence of a D-band originating from sharp folds in the graphene as opposed to from graphene cracks and edges. As can be seen from Figure 4a,b, the D′-band intensity (the shoulder of the G-band) varies with respect to that of the D-band as functions of the polarization angle. The strong polarization dependence as well as the 2-fold symmetry of the D-bands is in clear contrast to that of the G-band and 2D-band with no observable polarization dependence (Figure 4d). The characteristic $\cos^2\theta$ dependence of the D-band intensity as shown in Figure 4c originates from both photon absorption and emission.[29]

The prominent polarization dependence of the D-bands combined with their location coinciding with the graphene folds is clear evidence that the graphene folds function as one-dimensional scattering centers giving rise to double-resonance D-bands. There is no physical reason that randomly located broken carbon bonds could lead to the polarization dependence with the observed 2-fold symmetry. Large-curvature sharp folds in graphene have been predicted by theory to lead to D-bands,[30] providing further support to the hypothesis. One important implication of this finding can be traced to the physical origin of D-bands with the associated electrostatic potential fluctuations[31] at the irregularities in graphene, in this case graphene folds. The atomically smooth linear shape of the potential fluctuation (as opposed to randomly placed point defects along the edge of lithographically defined graphene) should function as a specular boundary

(as opposed to a diffuse boundary), ensuring the preservation of momentum and phase of the electrons.

As is evident, the interests in graphene−plasmonic surface interaction go beyond simple enhancement of graphene Raman signals. The possibility of placing graphene over nanostructured metal surfaces could serve as a way to tailor the biochemical properties of a plasmonic surface from conventional metallic ones to biocompatible carbon (graphitic) surfaces. Finally, configurational modification of graphene including the folds near the atomically sharp apex of the Au tipped surfaces holds the promise of transistor channels free of undesirable edge disorders.[32]

CONCLUSION

We report the experimental observation of a giant enhancement of graphene Raman signals (of up to 10^7) from graphene on plasmonic surfaces of Au nanopyramids (tips) with clear spectral selectivity, a signature of resonant effects. We present experimental evidence pointing to a new origin of graphene D-bands from spatial inhomogeneity in the graphene sheets, opening a new pathway to tailoring phonon and potentially electronic band structures of graphene for device applications such as biosensing and photodetection with drastically enhanced performance.

EXPERIMENTAL METHODS

Au Nanopyramid Fabrication. The periodic Au nanopyramid structure with tunable size and sharpness can be fabricated by a wafer-scale bottom-up templating technology (see details in the Supporting Information). Periodic inverted silicon pyramidal pits, which are templated from close-packed monolayer colloidal crystals prepared by a simple spin-coating technology, are employed as reusable structural templates to replicate arrays of gold nanopyramids with nanoscale sharp tips.

Micro-Raman Spectroscopy. Micro-Raman spectra and mapping of graphene, as well as the D-band polarization dependence measurements, were carried out using a Renishaw inVia Raman spectroscope under ambient conditions. The laser excitation wavelengths are 488, 514, and 633 nm from a diode-pumped solid-state laser and a He−Ne laser. The power of the lasers was kept at 1.5 mW to avoid sample heating. The laser spot size was ~0.5 μm. We used a 100× objective (numerical aperture 0.90). Spectral analysis was accomplished with a 1800 lines per mm grating. The spectroscope is equipped with a high-speed encoded stage that enables shift of samples in XYZ directions at nanometer steps. The nominal spatial resolution of the inVia Raman microscope is 100 nm. The spatially resolved Raman mapping data are achieved by Raman imaging with ~0.2 μm steps in the X and Y directions. The Raman imaging data were processed using WiRE 3.2 Raman software.

Conflict of Interest: The authors declare no competing financial interest.

Acknowledgment. The authors acknowledge the support of the FENA Focus Center, one of six research centers funded under the Focus Center Research Program (FCRP), a Semiconductor Research Corporation entity. P.W. and Y.H.X. would like to thank Dr. Wolfgang Mehr of IHP for his encouragement and facilitating the experiments, Dr. Grzegorz Lupina for helping with the experiments, and Grzegorz Kozlowski and Gunther Lippert of IHP for their help with instruction regarding Raman spectroscopy. Y.H.X. acknowledges the support of the Alexander von Humboldt Research Award.

Supporting Information Available: Description of Au nanopyramid fabrication; CVD synthesis and transfer of single-layer graphene; spatially resolved Raman spectra; and polarization dependence measurements. This material is available free of charge *via* the Internet at http://pubs.acs.org.

REFERENCES AND NOTES

1. Lee, C. G.; Wei, X. D.; Kysar, J. W.; Hone, J. Measurement of the Elastic Properties and Intrinsic Strength of Monolayer Graphene. *Science* **2008**, *321*, 385–388.
2. Neto, A. H. C.; Guinea, F.; Peres, N. M. R.; Novoselov, K. S.; Geim, A. K. The Electronic Properties of Graphene. *Rev. Mod. Phys.* **2009**, *81*, 109–162.
3. Bonaccorso, F.; Sun, Z.; Hasan, T.; Ferrari, A. C. Graphene Photonics and Optoelectronics. *Nat. Photonics* **2010**, *4*, 611–622.
4. Nair, R. R.; Blake, P.; Grigorenko, A. N.; Novoselov, K. S.; Booth, T. J.; Stauber, T.; Peres, N. M. R.; Geim, A. K. Fine Structure Constant Defines Visual Transparency of Graphene. *Science* **2008**, *320*, 1308.
5. Pumera, M. Graphene in Biosensing. *Mater. Today* **2011**, *14*, 308–315.
6. Rust, M. J.; Bates, M.; Zhuang, X. W. Sub-Diffraction Limit Imaging by Stochastic Optical Reconstruction Microscopy (STORM). *Nat. Methods* **2006**, *3*, 793.
7. Xia, F. N.; Mueller, T.; Lin, Y. M.; Valdes-Garcia, A.; Avouris, P. Ultrafast Graphene Photodetector. *Nat. Nanotechnol.* **2009**, *4*, 839–843.
8. Echtermeyer, T. J.; Britnell, L.; Jasnos, P. K.; Lombardo, A.; Gorbachev, R. V.; Grigorenko, A. N.; Geim, A. K.; Ferrari, A. C.; Novoselov, K. S. Strong Plasmonic Enhancement of Photovoltage in Graphene. *Nat. Commun.* **2011**, *2*, 458.
9. Liu, Y.; Cheng, R.; Liao, L.; Zhou, H. L.; Bai, J. W.; Liu, G.; Liu, L. X.; Huang, Y.; Duan., X. F. Plasmon Resonance Enhanced Multicolour Photodetection by Graphene. *Nat. Commun.* **2011**, *2*, 579.
10. Mueller, T.; Xia, F. N.; Avouris, P. Graphene Photodetectors for High-Speed Optical Communications. *Nat. Photonics* **2010**, *4*, 297–301.
11. Schedin, F.; Lidorikis, E.; Lombardo, A.; Kravets, V. G.; Geim, A. K.; Grigorenko, A. N.; Novoselov, K. S.; Ferrari, A. C. Surface-Enhanced Raman Spectroscopy of Graphene. *ACS Nano* **2010**, *4*, 5617–5626.
12. Schuller, J. A.; Barnard, E. S.; Cai, W. S.; Jun, Y. C.; White, J. S.; Brongersma, M. L. Plasmonics for Extreme Light Concentration and Manipulation. *Nat. Mater.* **2010**, *9*, 193–204.
13. Stöckle, R. M.; Suh, Y. D.; Deckert, V.; Zenobi, R. Nanoscale Chemical Analysis by Tip-Enhanced Raman Spectroscopy. *Chem. Phys. Lett.* **2000**, *318*, 131–136.
14. Sun, K.; Lee, J. Y.; Li, B. Y.; Liu, W.; Miao, C. Q.; Xie, Y. H.; Wei, X. Y.; Russell, T. P. Fabrication and Field Emission Study of Atomically Sharp High-Density Tungsten Nanotip Arrays. *J. Appl. Phys.* **2010**, *108*, 036102–036104.
15. Li, X. S.; Cai, W. W.; An, J. H.; Kim, S. Y.; Nah, J. H.; Yang, D. X.; Piner, R.; Velamakanni, A.; Jung, I. H.; Tutuc, E.; *et al.* Large-Area Synthesis of High Quality and Uniform Graphene Films on Cu Foils. *Science* **2009**, *324*, 1312–1314.
16. Li, X. S.; Cai, W.; Borysiak, M.; Han, B.; Chen, D.; Piner, R. D.; Colombo, L.; Ruoff, R. S. Transfer of Large-Area Graphene Films for High-Performance Transparent Conductive Electrodes. *Nano Lett.* **2009**, *9*, 4359–4363.
17. Bae, S.; Kim, H.; Lee, Y.; Xu, X.; Park, J. S.; Zheng, Y.; Balakrishnan, J.; Lei, T.; Kim, H. R.; Song, Y. I.; *et al.* Roll-to-Roll Production of 30-Inch Graphene Films for Transparent Electrodes. *Nat. Nanotechnol.* **2010**, *5*, 574–578.
18. Ferrari, A. C.; Meyer, J. C.; Scardaci, V.; Casiraghi, C.; Lazzeri, M.; Mauri, F.; Piscanec, S.; Jiang, D.; Novoselov, K. S.; Roth, S.; *et al.* Raman Spectrum of Graphene and Graphene Layers. *Phys. Rev. Lett.* **2006**, *97*, 187401.

19. Anker, J. N.; Hall, W. P.; Lyandres, O.; Shah, N. C.; Zhao, J.; Van Duyne, R. P. Biosensing with Plasmonic Nanosensors. *Nat. Mater.* **2008**, *7*, 442–453.
20. Moskovits, M. Surface-Enhanced Spectroscopy. *Rev. Mod. Phys.* **1985**, *57*, 783–826.
21. Jensen, L.; Aikens, C. M.; Schatz, G. C. Electronic Structure Methods for Studying Surface-Enhanced Raman Scattering. *Chem. Soc. Rev.* **2008**, *37*, 1061–1073.
22. Kerker, M. Electromagnetic Model for Surface-Enhanced Raman Scattering (SERS) on Metal Colloids. *Acc. Chem. Res.* **1984**, *17*, 271–277.
23. Sood, A. K.; Gupta, R.; Asher, S. A. Origin of the Unusual Dependence of Raman D Band on Excitation Wavelength in Graphite-Like Materials. *J. Appl. Phys.* **2001**, *90*, 4494–4497.
24. Cançado, L. G.; Takai, K.; Enoki, T.; Endo, M.; Kim, Y. A.; Mizusaki, H.; Jorio, A.; Coelho, L. N.; Magalha~Es-Paniago, R.; Pimenta, M. A. General Equation for the Determination of the Crystallite Size L_a of Nanographite by Raman Spectroscopy. *Appl. Phys. Lett.* **2006**, *88*, 3106–3109.
25. Ferrari, A. C.; Robertson, J. Resonant Raman Spectroscopy of Disordered, Amorphous, and Diamond-Like Carbon. *Phys. Rev. B* **2001**, *64*, 075414–075426.
26. Ozbay, E. Plasmonics: Merging Photonics and Electronics at Nanoscale Dimensions. *Science* **2006**, *311*, 189–193.
27. Graf, D.; Molitor, F.; Ensslin, K.; Stampfer, C.; Jungen, A.; Hierold, C.; Wirtz, L. Spatially Resolved Raman Spectroscopy of Single- and Few-Layer Graphene. *Nano Lett.* **2007**, *7*, 238–242.
28. Jin, M. L.; Pully, V.; Otto, C.; van den Berg, A.; Carlen, E. T. High-Density Periodic Arrays of Self-Aligned Subwavelength Nanopyramids for Surface-Enhanced Raman Spectroscopy. *J. Phys. Chem. C* **2010**, *114*, 21953–21959.
29. Gupta, A. K.; Russin, T. J.; Gutierrez, H. R.; Eklund, P. C. Probing Graphene Edges *via* Raman Scattering. *ACS Nano* **2009**, *3*, 45–52.
30. Gupta, A. K.; Nisoli, C.; Lammert, P. E.; Crespi, V. H.; Eklund, P. C. Curvature-Induced D-Band Raman Scattering in Folded Graphene. *J. Phys.: Condens. Matter* **2010**, *22*, 334205.
31. Pimenta, M. A.; Dresselhaus, G.; Dresselhaus, M. S.; Cançado, L. G.; Jorio, A.; Saito, R. Studying Disorder in Graphite-Based Systems by Raman Spectroscopy. *Phys. Chem. Chem. Phys.* **2007**, *9*, 1276–1291.
32. Nakada, K.; Fujita, M.; Dresselhaus, G.; Dresselhaus, M. S. Edge State in Graphene Ribbons: Nanometer Size Effect and Edge Shape Dependence. *Phys. Rev. B* **1996**, *54*, 24.